Catalysis Science & Technology

ROYAL SOCIETY OF CHEMISTRY

PAPER

View Article Online
View Journal | View Issue

Cite this: *Catal. Sci. Technol.*, 2023, **13**, 7123

Heterogeneous Pt-catalyzed transfer dehydrogenation of long-chain alkanes with ethylene†

Tim de la Croix, [a] Nathalie Claes, [b] Samuel Eyley, [c] Wim Thielemans, [c] Sara Bals [b] and Dirk De Vos *[a]

The dehydrogenation of long-chain alkanes to olefins and alkylaromatics is a challenging endothermic reaction, typically requiring harsh conditions which can lead to low selectivity and coking. More favorable thermodynamics can be achieved by using a hydrogen acceptor, such as ethylene. In this work, the potential of heterogeneous platinum catalysts for the transfer dehydrogenation of long-chain alkanes is investigated, using ethylene as a convenient hydrogen acceptor. Pt/C and Pt–Sn/C catalysts were prepared *via* a simple polyol method and characterized with CO pulse chemisorption, HAADF-STEM, and EDX measurements. Conversion of ethylene was monitored *via* gas-phase FTIR, and distribution of liquid products was analyzed *via* GC-FID, GC-MS, and 1H-NMR. Compared to unpromoted Pt/C, Sn-promoted catalysts show lower initial reaction rates, but better resistance to catalyst deactivation, while increasing selectivity towards alkylaromatics. Both reaction products and ethylene were found to inhibit the reaction significantly. At 250 °C for 22 h, TON up to 28 and 86 mol per mol Pt were obtained for Pt/C and $PtSn_2$/C, respectively, with olefin selectivities of 94% and 53%. The remaining products were mainly unbranched alkylaromatics. These findings show the potential of simple heterogeneous catalysts in alkane transfer dehydrogenation, for the preparation of valuable olefins and alkylaromatics, or as an essential step in various tandem reactions.

Received 16th March 2023,
Accepted 10th October 2023

DOI: 10.1039/d3cy00370a

rsc.li/catalysis

Introduction

The catalytic dehydrogenation of cheap and abundant alkanes to form valuable olefins and aromatics has been a major focus of catalysis research for decades, as olefins are a versatile feedstock for further synthesis of numerous chemicals and materials. Given the undeniable importance of this reaction, it is no surprise that many different approaches exist, including direct alkane dehydrogenation, oxidative dehydrogenation, and transfer dehydrogenation.[1–4]

Direct dehydrogenation of alkanes is widely applied in industry, for instance for the on-purpose production of propylene from propane. These processes typically use either supported chromium oxide or supported platinum catalysts. Although chromium catalysts have become less widespread due to their high toxicity, they are still used in the Catofin process by Lummus.[5–7] Notable Pt-based direct dehydrogenation processes include the UOP Oleflex process, utilizing a Pt-Sn catalyst supported on an alumina support and promoted with an alkali metal,[1,8] the Uhde STAR process, consisting of Pt–Sn supported on zinc-calcium aluminate,[1,9] and the Linde/BASF PDH process, which switched from a chromia/alumina system to the current Pt–Sn supported on zirconia.[1,10] Considering the high cost of platinum, significant research focuses on non-noble metal catalyzed dehydrogenation, for example based on nickel, but the lower productivity of these systems has thus far prevented their application.[11–13] A major limitation of the direct alkane dehydrogenation is the high endothermicity of the reaction, requiring very high temperatures (550–600 °C for propane dehydrogenation), which can lead to significant side reactions like cracking and coke formation. Processes for the dehydrogenation of longer alkanes (C_{10}–C_{14}) use similar catalysts, but are usually operated at lower temperatures (450–500 °C) and lower conversions (10–20%) to prevent excessive side reactions.[14]

Oxidative alkane dehydrogenation uses an oxidant, typically oxygen, to effectively remove thermodynamic limitations of the alkane dehydrogenation, producing water

[a] *Department of Microbial and Molecular Systems, Centre for Membrane Separations, Adsorption, Catalysis and Spectroscopy for Sustainable Solutions (cMACS), KU Leuven, 3001 Leuven, Belgium. E-mail: dirk.devos@kuleuven.be*
[b] *Electron Microscopy for Materials Science (EMAT) and NANOLab Center of Excellence, University of Antwerp, 2020 Antwerp, Belgium*
[c] *Sustainable Materials Lab, Department of Chemical Engineering, KU Leuven, Campus Kulak Kortrijk, 8500 Kortrijk, Belgium*

† Electronic supplementary information (ESI) available. See DOI: https://doi.org/10.1039/d3cy00370a

as a by-product instead of hydrogen. Catalysts typically consist of reducible metal oxides, often vanadium oxide, although recently boron nitride and other boron-containing materials were shown to be effective catalysts as well.[3,15,16] Despite favorable thermodynamics, high operating temperatures up to 800 °C are still required. Others have shown that CO_2 may also act as a mild oxidant, forming CO and H_2O alongside olefins, however, this reaction is still highly endothermic and requires high operating temperatures.[17] For longer alkanes, oxidative processes may not be viable, due to autoxidation to peroxides, or even auto-ignition at temperatures well below typical reaction temperatures.

Transfer dehydrogenations take a similar approach to circumvent thermodynamic limitations, by coupling the endothermic dehydrogenation reaction to the exothermic hydrogenation of a sacrificial alkene. Research on transfer dehydrogenation has so far been limited almost entirely to homogeneous catalysts, with so-called 'pincer'-complexes of iridium as the most common catalyst type since the work of Jensen *et al.* in 1996.[18] Countless variations on this original PCP-pincer ligand have been proposed and tested in the transfer dehydrogenation reaction.[2,19,20] The major advantage of these systems is that reaction temperatures can be reduced to 150–250 °C, while excellent turnover numbers can still be obtained. Operating in the liquid phase, these systems can also be applied easily to long-chain alkanes and even polyolefins, in contrast to typical dehydrogenation processes. However, synthesis and recovery of the homogeneous catalysts can be difficult and expensive, which may limit their application in large-scale operations. Furthermore, while examples exist of catalysts that utilize widely available ethylene as the sacrificial olefin,[21,22] the majority of catalysts have only been tested with less ideal hydrogen acceptors, such as *tert*-butyl ethylene, and ethylene is likely to cause rapid catalyst deactivation in many cases.[21,23]

Catalytic dehydrogenation of longer alkanes and polyolefins that are incompatible with classic approaches is more relevant than ever, in particular due to a rise in research on catalytic upcycling of waste polyolefins. A wide variety of polyolefin upcycling processes have been proposed in recent years. Pyrolysis involves treating the polymer at high temperatures, either with or without catalyst, yielding a mixture of gases, char, and liquid alkanes, olefins, and aromatics.[24–26] Although this method is straightforward, the high energy requirement and low product selectivity may limit the commercial potential of pyrolysis processes. Alternatively, hydrogenolysis using supported Pt or Ru catalysts has been proposed as a way to convert polyolefins into waxes and fuels.[27–31] While these products may have significant value, fuels are inevitably burned and do not contribute to a circular economy. The same can be said for alkane metathesis, which consists of tandem (de) hydrogenation and olefin metathesis reactions using homogeneous or heterogeneous catalysts.[32,33] Since the olefin products are re-hydrogenated after metathesis, only saturated fuels and waxes are produced. In contrast, a tandem dehydroaromatization/hydrogenolysis process was proposed, using only a Pt/Al_2O_3 catalyst.[34] The desired final products of this reaction are long-chain alkylaromatics, which find uses in the production of surfactants, for example. Alternatively, a bromination/debromination process was shown to yield partially dehydrogenated polyethylene, which could be decomposed *via* ethenolysis.[35] Most recently, dehydrogenation and transfer dehydrogenation reactions were proposed for the partial dehydrogenation of polyethylene, to allow for decomposition to propylene using tandem isomerization/ethenolysis reactions. In these processes, appreciable yields were obtained with olefin-terminated polyethylene, but a saturated polyethylene partially dehydrogenated over $Pt/\gamma\text{-}Al_2O_3$ in the presence of ethylene yielded only 1 wt% propylene, likely due to poor performance of the transfer dehydrogenation.[36,37]

In many of these processes, hydrogen transfer reactions take place on heterogeneous platinum catalysts. Despite this, to our knowledge, no thorough investigation of the platinum-catalyzed transfer dehydrogenation of alkanes as an isolated reaction has been performed. In this work, the transfer dehydrogenation of long-chain alkanes using simple heterogeneous catalysts is investigated, as an alternative to homogeneous Ir-pincer systems, using the tetradecane/ethylene couple as a model system.

Experimental

Materials

Activated carbon (Norit GSX) and tin(II)chloride ($SnCl_2$, anhydrous, >98%) were purchased from Fischer Scientific. Chloroplatinic acid hexahydrate ($H_2PtCl_6{\cdot}6H_2O$, 37.5% Pt) and platinum on alumina (5 wt%) were purchased from Merck. Ethylene glycol (>99.5%) and platinum on carbon (5 wt%) were obtained from Acros Organics. *n*-Tetradecane (>99%) was purchased from TCI Europe. Ethylene (>99.5%) was obtained from Air Liquide. Products were used as received without further purification.

Catalyst preparation

Carbon-supported Pt–Sn catalysts were prepared *via* a simple one-pot polyol method. $SnCl_2$ and HCl were first dissolved in ethylene glycol. H_2PtCl_6 was added to this mixture as an aqueous solution (0.1 g ml^{-1}). The typical platinum concentration was 2.5 mM. HCl concentration was kept equal to the platinum concentration, and Sn was added in different ratios. Activated carbon was added under constant stirring to reach a nominal Pt loading of 5 wt%. After stirring for 2 hours, the mixture was heated in an oil bath to 140 °C and held at this temperature for 3 h before it was allowed to cool to room temperature. The resulting solid catalyst was recovered by filtration and rinsed with distilled water until the pH of the filtrate was neutral, then dried in an oven at 60 °C overnight.

Catalyst characterization

CO chemisorption. Pt dispersions were determined *via* CO pulse chemisorption on a ChemBET pulsar instrument. Catalyst samples were placed in a U-shaped quartz tube and activated in flowing hydrogen at 250 °C for 1 h. Adsorbed hydrogen was then removed in flowing He at 250 °C for 1 h, before cooling to room temperature. The activated sample was then subjected to automated CO pulse chemisorption analysis at 40 °C. CO adsorption was quantified using a thermal conductivity detector. The Pt dispersion was calculated assuming a CO/surface Pt stoichiometry of 1. Equivalent particle sizes were calculated assuming spherical particles.

N_2 Physisorption. Texture analysis of catalysts was performed *via* physisorption of N_2 at 77 K. Samples were degassed at 200 °C for 6 hours prior to analysis.

The Brunauer–Emmett–Teller (BET) method was used to determine specific surface areas. The Barett–Joyner–Halenda method was used to determine pore size distributions. Isotherms and textural characteristics are provided as ESI† (Fig. S1 and Table S1)

NH_3 TPD. Temperature programmed desorption of ammonia to determine catalyst acidity was performed using a ChemBET pulsar instrument. Catalyst samples were activated as for CO chemisorption. The activated samples were then saturated with NH_3 at ambient temperature in flowing NH_3 for 30 minutes. Weakly adsorbed NH_3 was removed in flowing He at 100 °C. TPD data was then collected from 100 °C to 600 °C at a heating rate of 10 °C min^{-1}. A baseline for each sample was obtained by the same procedure without the NH_3 saturation step. The negative signals above 300 °C are ascribed to Pt-catalyzed decomposition of NH_3 and subsequent desorption of H_2.[38] For this reason, only the initial desorption peaks were used to determine acid site density.

TEM imaging. Carbon supported Pt and Pt–Sn catalysts were drop-casted (3 μl) on a holey carbon TEM grid. High Angle Annular Dark-Field Scanning Transmission Electron Microscopy (HAADF-STEM) were carried out on a Tecnai Osiris (Thermo Fisher Scientific) TEM operated at 200 kV. High resolution STEM images were acquired using an aberration-corrected cubed Titan (Thermo Fisher Scientific) operated at 300 kV. The Energy Dispersive X-ray spectroscopy (EDX) measurements were performed using a ChemiSTEM system and analyzed using the Bruker Esprit software. HAADF-STEM images and EDX maps were acquired with respectively 50 pA and 150 pA beam current.

XPS analysis. XPS measurements were performed on a Kratos Axis Supra photoelectron spectrometer employing a monochromated Al Kα (1486.7 eV, 120 W) X-ray source, hybrid (magnetic/electrostatic) optics and a hemisphere analyser. The analyser was operated in fixed analyser transmission (FAT) mode with survey scans taken at a pass energy of 160 eV and high-resolution scans at a pass energy of 20 eV. The samples were measured at normal emission, in electrical contact with the spectrometer. The binding energy scale was referenced to Ag $3d_{5/2}$ at 368.21 eV measured on the same day as the analysis and under the same conditions.

Spectra were processed using CasaXPS (2.3.26rev1.2Q). Elemental quantification was performed using relative sensitivity factors derived from Scofield cross-sections, corrected for the angular distribution of photoelectrons (γ = 60°) and the electron attenuation length according to Seah.[39] The instrument transmission function was characterized with a NPL transmission function.[40] The resulting atomic concentrations represent the homogeneous equivalent composition and do not take into account the nanostructure of the material.

Transfer dehydrogenation

Dehydrogenation reactions were conducted in a 50 mL stainless steel Parr reactor. In a typical reaction, 10 mL of *n*-tetradecane was added to the catalyst without additional solvent and the reactor was purged with high-purity N_2 and H_2. The mixture was stirred at 350 rpm and heated to the reaction temperature under a hydrogen atmosphere to activate the catalyst, then purged with nitrogen. Ethylene was then added to the reactor to reach the desired partial pressure, typically between 0.5 and 2 bar. No further ethylene dissolution was observed, indicating the liquid phase was saturated with ethylene. Alternatively, ethylene was continuously fed into the reactor with a mass flow controller, while keeping the reactor at constant pressure *via* a backpressure regulator. Simplified diagrams of both set-ups are provided as ESI† (Fig. S3). Reaction times are reported starting from the addition of ethylene. To stop the reaction, the reactor was quenched in an ice-bath.

Product analysis

Gas phase samples were taken at several points during the reaction and the composition was analyzed *via* Fourier Transform Infrared Spectroscopy (FTIR). The gas samples were injected into a constant nitrogen flow and analyzed with a Gasmet DX4000 FTIR detector. The gas-phase composition was determined from the FTIR spectrum using Calcmet software. Ethylene conversion was then calculated from the observed ethane/ethylene ratio in each sample. Ethylene consumption (in mmol) is calculated based on an estimated headspace volume of 58 ml.

Liquid products were quantified *via* GC-FID, on a DB-FFAP capillary column. The oven program was adjusted to allow separation of tetradecenes from tetradecane. Concentrations of C_{14} products are approximated using a simple area% approach, which was confirmed to be a good approximation using authentic samples of *n*-tetradecane, 1-tetradecene, and 1-phenyloctane. Differences in the FID response factors were found to be below 5% within the relevant concentration range.

^{1}H-NMR spectra were also collected for several samples to verify results as obtained by GC. The liquid product, dissolved in $CDCl_3$, was analyzed in a Bruker Avance III HD 400 MHz spectrometer equipped with a 5 mm PABBO BB

SmartProbe, using the zg30 pulse program. The spectrum was processed using Bruker TopSpin software.

Products were further identified *via* GC-MS, using a VF-WAXms column for separation. Mass spectra obtained for the major products were compared to the NIST11 library for identification.

Results and discussion

Platinum catalysts were selected from a preliminary screening of several commercially available catalysts for their activity in the transfer dehydrogenation of *n*-tetradecane with ethylene at 250 °C and 1 bar ethylene. Ru/C and Ni/SiO_2 were quickly disqualified, as significant hydrogenolysis reactions were observed, producing undesired methane. The activity of Ru and Ni for hydrogenolysis of alkanes is well-known in literature.[13,28,41] Pd/C and Pt/C both showed potential, with good selectivity towards tetradecenes, and only C_{14}-alkylaromatics as major by-products, but with significantly higher activity for Pt/C. Pt/C was thus selected as the reference material for further investigations.

Ethylene consumption, measured at several points in the reaction, and product analysis after 6 h for both 5 wt% Pt/C and a commercially available 5 wt% Pt/Al_2O_3 are shown in Fig. 1. In the absence of catalyst, only traces of ethane and tetradecenes were detected. In a reaction containing Pt/C, but no ethylene, no gas phase organic components were observed on FTIR and only trace amounts of tetradecenes were detected in the product. This shows that the presence of a hydrogen acceptor, in this case in the form of a sacrificial alkene, is crucial to the reaction under these conditions. The time profile of ethylene consumption shows a severe decrease in activity after the first hour for both catalysts, but more than two times higher activity for Pt/C than for Pt/Al_2O_3. Therefore, Pt/Al_2O_3 was not further investigated. Textural characteristics, as determined by N_2 physisorption (Fig. S1† and Table S1), show notably larger pores and a lower specific surface area for Pt/Al_2O_3 compared to carbon-supported catalysts. Given the very similar Pt dispersion as determined by CO chemisorption, and the identical pretreatment under H_2, the large difference in activity between Pt/C and Pt/Al_2O_3 is expected to be due to particle/support interactions, which alter the electronic state of the platinum particles.[42,43] Alternatively, the higher surface acidity of the alumina support compared to carbon[44,45] may cause coking and other side reactions, leading to more rapid deactivation. NH_3 TPD (Fig. S2†) indeed shows more and stronger acid sites for the Al_2O_3-supported catalyst, but acidity for both materials is almost negligible. Furthermore, no aromatics, branched hydrocarbons, or other evidence of increased acid-catalyzed reactions were found in the liquid phase. Results are consistent with the assumption that practically all hydrogen produced in dehydrogenation and dehydroaromatization reactions is consumed in the ethylene hydrogenation, with only minor deviations in the hydrogen balance of the reaction. Typical FTIR spectra, gas chromatograms, and GC-MS and ^{1}H-NMR analyses are provided as ESI† (Fig. S4–S8†). Aside from olefins and alkylaromatics, traces of dienes or cyclic alkenes were also observed as a number of very small peaks, but these were not quantified. Trienes or cyclic dienes were not detected and are expected to be converted rapidly to alkylaromatics. Olefins appear to be present as a thermodynamic mixture of linear tetradecenes, with only minor amounts of 1-tetradecene. This is to be expected in the presence of small amounts of hydrogen on a noble metal catalyst, with isomerization occurring through a half-hydrogenated state, as in the Horiuti–Polanyi mechanism[46,47] similarly, aromatics appear to be almost exclusively unbranched *o*-dialkylaromatics, with minor amounts of 1-phenyloctane. No evidence for branching or cracking reactions was observed, likely due to the limited acidity of the carbon support and the relatively mild reaction conditions.

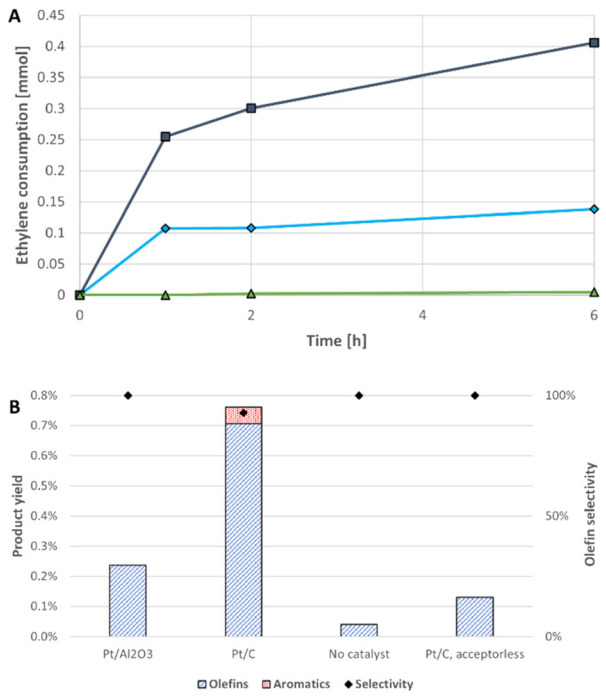

Fig. 1 A) Ethylene consumption over 5 wt% Pt/C (■); 5 wt% Pt/Al_2O_3 (♦); without catalyst (▲). B) GC yield of C_{14} products (olefins and alkylaromatics) and selectivity towards olefins. Reaction conditions: 0.05 mmol Pt in 10 ml *n*-tetradecane (38.4 mmol), 1 bar ethylene at *t* = 0 (1.15 mmol), 250 °C, 6 h.

Inspired by industrially applied propane dehydrogenation processes such as STAR and OleFlex,[1,8,9] Sn-promoted Pt catalysts were prepared on an activated carbon support, and tested under identical conditions, but with reaction times up to 22 hours. The results of these reactions are shown in Fig. 2. The behavior of these Pt–Sn catalysts is clearly distinct from that of unpromoted Pt/C. The observed dehydrogenation rate is essentially constant in the first six hours of the reaction, compared to the rapid deactivation of the Pt/C. Indeed, Pt–Sn catalysts are known to show decreased catalyst deactivation in alkane dehydrogenation reactions, due to both electronic and geometric effects. In propane dehydrogenation, Sn promotes the desorption of propylene[48,49] and olefin adsorption studies on model

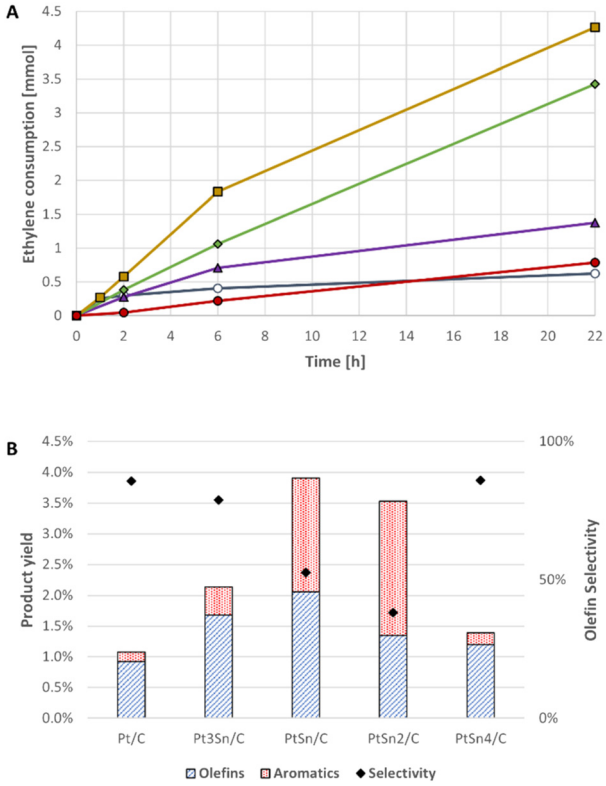

Fig. 2 A) Ethylene consumption over 5 wt% Pt/C (○); 5 wt% Pt_3Sn/C (▲); 5 wt% PtSn/C (♦); 5 wt% $PtSn_2$/C (■); 5 wt% $PtSn_4$/C (●). B) GC yield of C_{14} products (olefins and alkylaromatics) and selectivity towards olefins. Reaction conditions: 0.05 mmol Pt in 10 ml *n*-tetradecane (38.4 mmol), 1 bar ethylene at t = 0 (1.15 mmol), 250 °C, 22 h.

surfaces clearly show improved molecular desorption of olefins on Pt–Sn alloys.[50] Indeed, many XPS and EXAFS studies indicate increased electron density on Sn-promoted Pt catalysts.[51–53] Note that, while initial ethylene pressure was always 1 bar, ethylene was added to the reactor when gas phase samples indicated ethylene would run out otherwise. These additions did not appear to significantly alter the reaction rate or deactivation behavior. Compared to the 6 hour reaction, selectivity on the Pt/C catalyst decreases slightly, which is to be expected from the higher olefin concentration and reaction time. The ethylene hydrogenation rate increases as the Sn : Pt ratio increases from 1/3 to 2, but decreases strongly as the ratio is further increased to 4. For $PtSn_2$/C, up to 4.3 mmol of ethylene was hydrogenated, or 86 mol per mol Pt. Under these conditions, only 12 mol per mol Pt) was hydrogenated over Pt/C. Unexpectedly, with increasing Sn : Pt ratio, selectivity shifts dramatically towards aromatics. This seems counterintuitive, as Sn is expected to promote desorption of tetradecenes. While under the particular conditions of this experiment, PtSn/C reaches the highest olefin yield, $PtSn_2$/C was chosen for further investigation and comparison to Pt/C, as the change in activity and selectivity towards aromatics appears to be most pronounced here. The slight deactivation of $PtSn_2$/C in the 6–22 h interval may be caused by relatively high product concentrations and insufficient ethylene to further drive the reaction. A control reaction using a mixture of Pt/C and SnO_2/Al_2O_3 showed no significant difference to Pt/C, indicating that the increased aromatization is indeed catalyzed by the Pt–Sn particles, rather than by isolated Sn or acid sites. NH_3 TPD (Fig. S2†) shows slightly stronger, but fewer acid sites for the $PtSn_2$/C catalyst, but this difference is unlikely to explain the major shift in selectivity. One possibility is that the Pt-Sn phase favors reversible adsorption of olefins, for example *via* weaker π-bonding and van der Waals interactions,[54,55] which may promote dehydrogenation of adjacent C–C bonds and subsequent aromatization. In contrast, unpromoted Pt may adsorb olefins *via* strong σ-bonds, which can lead to the formation of alkylidyne species and elemental carbon, deactivating the catalyst.

Pt/C and $PtSn_2$/C were analyzed *via* HAADF-STEM and EDX (Fig. 3), XPS (Fig. 4, Table 1), and CO chemisorption (Table 2) before and after reaction. Fresh samples were reduced in hydrogen at 250 °C and kept under nitrogen

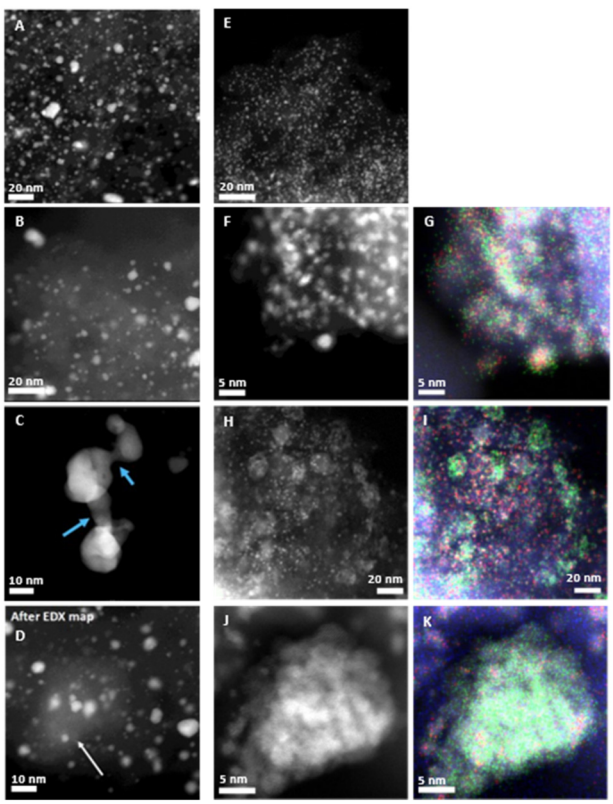

Fig. 3 HAADF-STEM and EDX (Pt = red, Sn = green, C = blue) imaging of 5 wt% Pt/C (A–D) and $PtSn_2C$ (E–K). A) 5 wt% Pt/C, fresh; B) 5 wt% Pt/C, post reaction; C) 5 wt% Pt/C, post reaction, signs of Pt sintering; D) 5 wt% Pt/C, post reaction, contrast is reduced by carbon contamination after EDX mapping; E) 5 wt% $PtSn_2$/C, fresh; F and G) 5 wt% $PtSn_2$/C, fresh, EDX map shows Pt-rich cores and Sn-rich shells; H and I) 5 wt% $PtSn_2$/C, post reaction, larger structures observed, EDX shows mainly Sn in these structures; J and K) $PtSn_2$/C, post reaction, higher magnification shows small Pt clusters on the larger Sn structures.

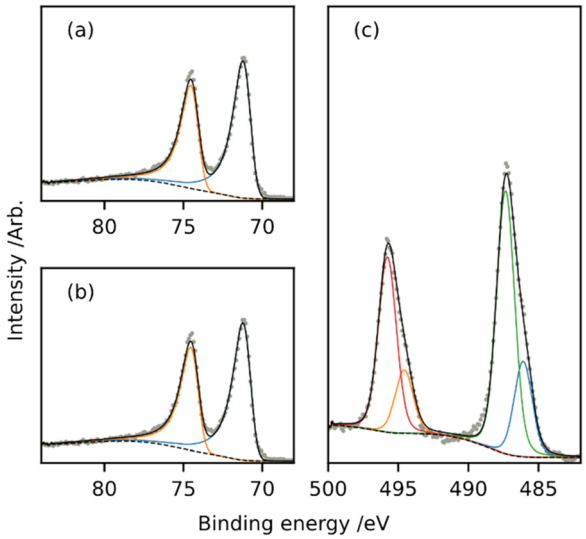

Fig. 4 (a) Pt 4f region of the XPS spectrum for Pt/C (b) Pt 4f region and (c) Sn 3d region of the XPS spectrum for $PtSn_2$/C.

before analysis. Post-reaction samples were washed with pentane and dried under nitrogen flow before analysis. pentane was chosen to remove tetradecane and soluble products, without removing potential carbon deposits from the Pt surface.

STEM-EDX analysis shows that Pt/C consists mainly of Pt particles around 2–3 nm in size, with some larger particles up to 15 nm. The average particle size is 3.22 nm (σ = 0.11 nm). After reaction, there are clear signs of sintering and the average particle size increases to 4.15 nm (σ = 0.16 nm). Interestingly, after EDX analysis, carbon contamination is observed in the sample. This may indicate the presence of adsorbed carbon atoms on the surface which formed a carbon layer upon exposure to the electron beam.

The $PtSn_2$/C catalyst is shown to consist of well-dispersed particles around 2 nm in size. Upon closer inspection, most particles appear to contain a Pt-rich core and Sn-rich shell, and no monometallic Pt particles are observed. The core–shell structure can be explained by the mild reduction in ethylene glycol at 140 °C, which only allows for reduction of the less noble Sn in the presence of Pt nuclei.[56] Additional Sn may be deposited as tin oxides. A few larger clusters consisting almost exclusively of Sn are observed. The 2 : 1 Sn : Pt ratio in this catalyst likely leads to an excess of Sn which agglomerates in these larger structures. After reaction, dispersion of Pt remains high, with minimal signs of sintering. However, more of the large Sn clusters appear, indicating that some of the Sn is mobile. These may be formed by excess Sn that is not stabilized in bimetallic particles, and might not affect the catalytic properties. The core-shell structure of the bimetallic particles remains intact and likely stabilizes the catalyst towards sintering. No carbon contamination is observed on this catalyst, despite identical post-reaction treatment, which may indicate that no residual carbon atoms were adsorbed to the surface.

XPS analysis of the catalysts shows only a single Pt species for both Pt/C and $PtSn_2$/C, corresponding to Pt(0) (70.9–71.2 eV). For the $PtSn_2$/C catalyst, two Sn species appear to be present. The species at higher binding energy (487.4 eV) is assigned to SnO_2, while the species at lower binding energy (486.1 eV) is tentatively assigned to SnO, as the binding energy is higher than would be expected for metallic Sn.[57,58] However, these oxidized states of Sn are typically almost indistinguishable by XPS. Another possibility is that this species corresponds to electron-deficient metallic Sn, for example through electron donation to adjacent Pt. Regardless, the majority of Sn in the catalyst is in an oxidized state. While it is possible that some additional oxidation occurred in ambient atmosphere during sample handling, Sn is not expected to be fully reduced at typical reduction conditions. The observed surface atomic ratio of Sn to Pt is 3.47, compared to the nominal ratio of 2 in the catalyst. This further supports a core/shell structure of the catalyst, as observed in TEM images. Additional XPS data is provided as supplementary information (Table S2†).

Table 1 XPS data for Pt/C and $PtSn_2$/C

Catalyst	Pt $4f_{7/2}$ binding energy (eV)	Sn $3d_{5/2}$ binding energy (eV)	Sn/Pt (atomic ratio at surface)
Pt/C	70.90	—	—
$PtSn_2$/C	71.16	487.35 (SnO_2, 74%) 486.09 (SnO, 26%)	3.47

Table 2 Pt dispersion and equivalent average particle size based on CO pulse chemisorption analysis

Sample	Pt dispersion	Equivalent particle size[a]	Particle size (TEM)
5 wt% Pt/C (fresh)	29%	3.9 nm	3.2 nm
5 wt% Pt/Al_2O_3 (fresh)	30%	3.8 nm	—
5 wt% $PtSn_2$/C (fresh)	13%	8.8 nm	~2 nm
5 wt% Pt/C (used)	10%	11 nm	4.1 nm
5 wt% $PtSn_2$ (used)	2.5%	45 nm	~2 nm

[a] Calculated assuming all Pt atoms on the exterior of particles are available for CO chemisorption in a 1 : 1 CO : Pt stoichiometry.

CO chemisorption data, summarized in Table 2, correspond well with the average particle size observed on STEM images for the fresh Pt/C catalyst. Dispersion of the Pt/Al_2O_3 catalyst is very similar, and is assumed to be representative of the average particle size. For $PtSn_2$/C, a large difference is obtained between particle size calculated from CO chemisorption and observed on STEM images. In the presence of Sn, a significant fraction of Pt atoms appear to be covered by Sn, leading to an actual CO/Pt stoichiometry below 1. Electronic effects may also decrease the affinity of CO for the surface. After reaction, CO chemisorption on both catalysts decreased significantly, despite relatively minor changes in particle size as observed on STEM images. For Pt/C, the likely cause is the presence of strongly adsorbed hydrocarbon species and elemental carbon on the Pt surface. For $PtSn_2$/C, the effect of carbon deposition is expected to be lower. However, the observed mobility of Sn during the reaction may lead to blocking of additional surface Pt, and a further decrease of the CO : Pt stoichiometry.

Kinetic experiments to determine the influence of temperature and ethylene pressure, were performed with both Pt/C and $PtSn_2$/C. For these experiments, reaction time was limited to 30 minutes, to avoid catalyst deactivation as much as possible. Shorter reaction times were not attempted as thermal equilibration and ethylene mixing and dissolution might reduce reproducibility of the reaction. Results at temperatures ranging from 220 °C to 260 °C are shown in Fig. 5. Both ethylene consumption and tetradecene production show good linearity in the Arrhenius plot. As expected, increasing the temperature increases catalyst activity for both catalysts. It is clear that the effect of temperature is much larger for $PtSn_2$/C than for Pt/C. Deviations from the expected hydrogen balance, that is, the ratio between ethylene hydrogenation and alkane dehydrogenation, are larger than in previous experiments, and specifically for Pt/C, a lower than expected C_{14}-olefin yield is observed, with greater deviations at lower temperatures. It is possible that, at the short reaction time, reactions that would otherwise be negligible have relatively large effects. The increase in ethylene hydrogenation that cannot be attributed to alkane dehydrogenation could for example arise from residual hydrogen on the activated catalyst, or from ethylene self-hydrogenation.[59] Small amounts of products may also remain adsorbed on the carbon-supported catalyst. These deviations also lead to somewhat different values for the apparent activation energy derived from the Arrhenius plot, leading to a significant margin of error. However, the error range is small compared to the difference between the catalysts. Specifically, the calculated apparent activation energy for Pt/C 60 ± 5 kJ mol^{-1}, while for $PtSn_2$/C an activation energy of 151 ± 5 kJ mol^{-1} is obtained. The large increase in activation energy for $PtSn_2$/C is consistent with DFT calculations that show that

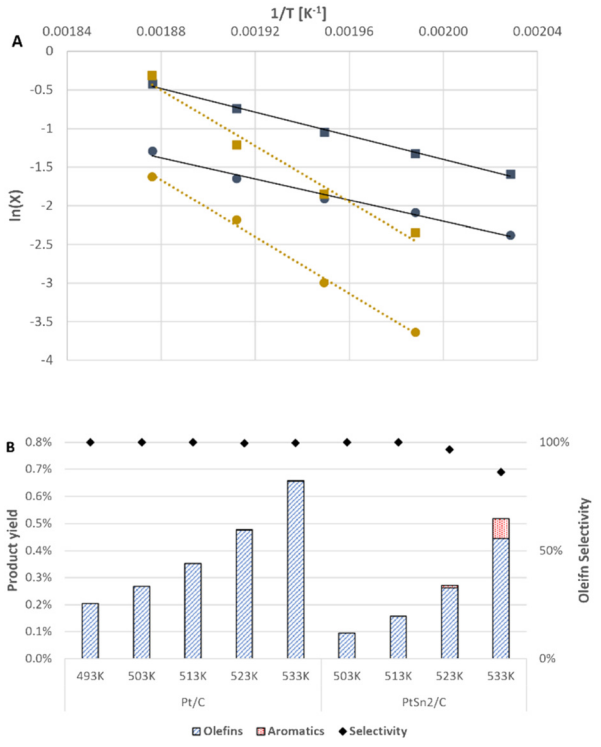

Fig. 5 A) Arrhenius plot for 5 wt% Pt/C (—) and 5 wt% $PtSn_2$/C (---), based on initial rate of ethylene hydrogenation (■) and initial rate of tetradecane dehydrogenation (●). B) GC yield of C_{14} products (olefins and alkylaromatics) and selectivity towards olefins at different temperatures. Reaction conditions: 0.05 mmol Pt in 10 ml *n*-tetradecane (38.4 mmol), 1 bar ethylene at t = 0 (1.15 mmol), 0.5 h.

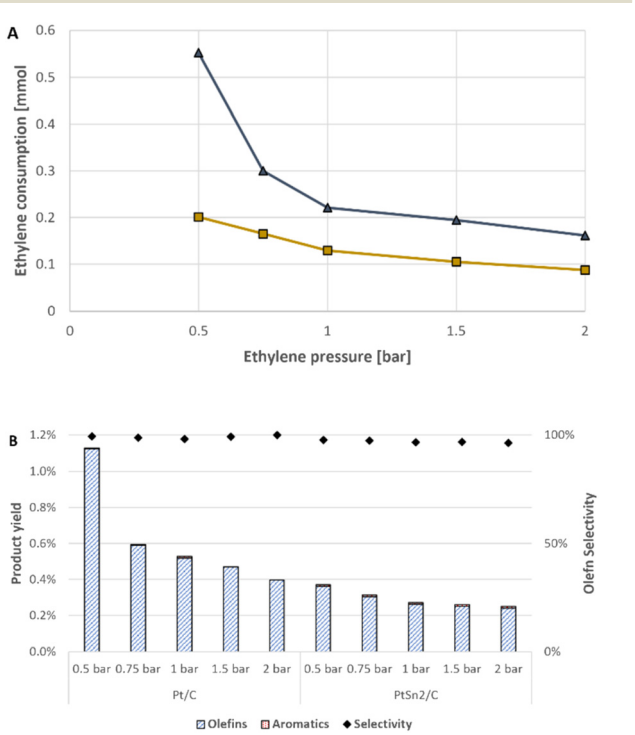

Fig. 6 A) Initial ethylene consumption at different initial ethylene pressures over 5 wt% Pt/C (▲) and 5 wt% $PtSn_2$/C (■). B) GC yield of C_{14} products (olefins and alkylaromatics) and selectivity towards olefins at different initial ethylene pressures. Reaction conditions: 0.05 mmol Pt in 10 ml *n*-tetradecane (38.4 mmol), 250 °C, 0.5 h.

promotion with Sn increases the activation energy for alkane and olefin adsorption.[48,49] The rate-limiting step in this reaction is most likely the difficult alkane adsorption through activation of a strong C–H bond. Despite a slight decrease in selectivity, increasing the temperature appears to be a valid method for increasing the reaction rate or decreasing catalyst loading, with no observed side reactions such as cracking or hydrogenolysis. For the purpose of this investigation, however, the reaction temperature is kept at 250 °C.

When investigating the effect of ethylene pressure (0.5–2 bar), Fig. 6 clearly shows adverse effects of increasing the pressure for both catalysts. The largest effect can be seen at low ethylene pressure over the Pt/C catalyst, where ethylene consumption and tetradecene production rates both increase by a factor of more than 2, as pressure is decreased from 1 to 0.5 bar. The $PtSn_2$/C catalyst appears to be less sensitive to changes in ethylene pressure, although a significant rate increase is still observed as pressure decreases. The negative effect of ethylene pressure can likely be understood in terms of both competitive adsorption with alkanes and catalyst deactivation *via* irreversible adsorption. On a platinum surface, ethylene is known to adsorb strongly in three-fold hollow Pt sites, as ethylidyne species. At high temperatures (>450 K), ethylidyne may undergo further dehydrogenation to carbon deposits. Sn-promoted catalysts may suppress the catalyst deactivation by ethylene through electronic effects, by reducing the adsorption energy of ethylene, and by geometric effects, by diluting the Pt surface, reducing the amount of three-fold hollow adsorption sites available for ethylidyne formation. However, much discussion still persists in literature on the exact nature of the promotion by Sn.[48,49,59–61] As with the temperature experiments, the measured ethylene consumption does not exactly match the observed olefin yield, although both values follow the same trends. Specifically, as pressure decreases, more ethylene appears to be consumed that cannot be linked directly to alkane dehydrogenation, likely due to residual hydrogen and/or ethylene self-hydrogenation. Overall, it is clear that the obtained results cannot be fitted with a simple power law for ethylene. When calculating the kinetic order of ethylene in the reaction for Pt/C, it varies from approximately −1.5 at low pressures (between 0.5 and 0.75 bar) to −0.5 at higher pressures (between 1.5 and 2 bar). For $PtSn_2$/C, these calculations yield an order of only −0.5 in both pressure intervals, based on ethylene hydrogenation rates. When calculating the order from the olefin yields, the values are generally similar for Pt/C, but the apparent order decreases to only −0.1 for $PtSn_2$/C, as very similar olefin yields are observed at 1 and 2 bar ethylene. At low pressures, an increase in ethylene pressure likely causes a significant increase in sites occupied by ethylene, ethylidyne, or carbon deposits, while further increases have less effect as preferential adsorption sites are depleted. Deposited cokes may also alter the electronic state of platinum, decreasing further carbon deposition.[62]

Based on this observed dependence of the reaction rate on the ethylene pressure, ethylene pressure should be kept low throughout the reaction to maintain high dehydrogenation rates and avoid catalyst deactivation.

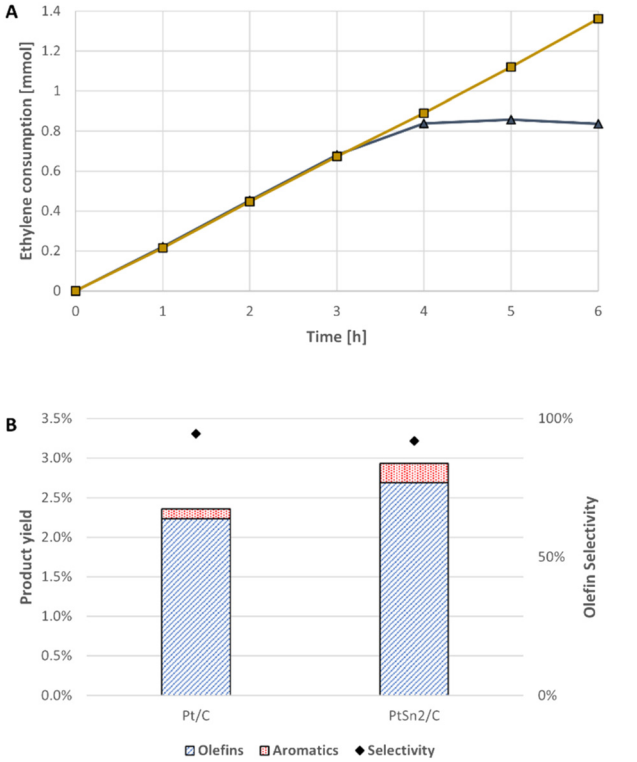

Fig. 7 A) Total ethylene consumption over 5 wt% Pt/C (▲) and 5 wt% $PtSn_2$/C (■), 0.2 bar ethylene (0.23 mmol) is added per hour. B) GC yield of C_{14} products (olefins and alkylaromatics) and selectivity towards olefins after 6 h. Reaction conditions: 0.05 mmol Pt in 10 ml *n*-tetradecane (38.4 mmol), 250 °C, 0.2 bar h^{-1} ethylene (0.23 mmol h^{-1}), 6 h.

Initially, this was accomplished by adding ethylene to the reactor stepwise, allowing the ethylene to be consumed at every interval. The result of these experiments, where 0.2 bar ethylene was added every hour, is shown in Fig. 7. In the first 3 hours, practically full conversion of ethylene into ethane was observed for both catalysts. After 4 hours, 9% residual ethylene was detected for Pt/C, and minimal further activity was observed in the remainder of the reaction. Compared to previous reactions, it appears that the stepwise dosing of ethylene may not only allow for high reaction rates due to low pressure, but could also prevent, or at least delay, catalyst deactivation. This may indicate that early catalyst deactivation is to a significant extent due to ethylene adsorption and to the formation of irreversibly adsorbed ethylidyne and carbon. Overall, up to 0.83 mmol ethylene (or 16.6 mol per mol Pt) was consumed in 4 hours in these conditions, compared to only 0.62 mmol (12.4 mol per mol Pt) in 22 h when 1 bar ethylene was simply added at the start of the reaction. For $PtSn_2$/C, all samples showed less than 5% residual ethylene, in accordance with previous reactions showing no significant deactivation in this timeframe. Remarkably, olefin selectivity for $PtSn_2$/C was much higher than anticipated at 91%, while a typical batch reaction

yielded only 70% selectivity towards olefins after 6 hours. The improved selectivity may be caused by adsorbed hydrogen on the catalyst, which is scavenged more slowly at low ethylene pressures and may inhibit sequential dehydrogenation and aromatization.

To further expand on the concept of gradually dosing ethylene, the reactor set-up was modified with a mass flow controller suitable for low ethylene flows. The reactor was kept at atmospheric pressure and the mass flow controller set to 0.1 ml_n min^{-1}, equivalent to 0.26 mmol h^{-1}, or 0.23 bar h^{-1}. Outlet tubing was flushed with nitrogen along with the reactor itself, to prevent oxygen from reaching the reactor, as the gas flow is very limited. Reactions lasted 22 hours, after which the gas-phase composition at the reactor outlet was determined (Table 3).

For Pt/C, only 10% ethylene conversion was observed at the end of the reaction, despite an overall conversion of ethylene of 24.5% over the full run. Although only qualitative, this difference indicates that activity was likely high at the start of the reaction, before severe deactivation occurred. For $PtSn_2$/C, 55% ethylene conversion was detected after 22 hours, very close to the calculated overall conversion. In contrast with Pt/C, this indicates that the reaction rate is likely quite stable during the reaction. The reaction with $PtSn_2$/C was repeated with an extended reaction time of 70 hours, after which only 30% ethylene conversion was still detected, compared to 43.5% overall conversion, indicating catalyst deactivation, but less severe than for Pt/C.

Analysis of the liquid products is shown in Fig. 8. Under these conditions, Pt/C reaches the highest olefin yields so far, with excellent selectivity towards tetradecenes (94%). Up to 28 mol per mol Pt) of ethylene was hydrogenated. $PtSn_2$/C also shows high dehydrogenation activity under these conditions, although selectivity towards olefins is only 66%. As shown in Fig. 2, however, selectivity for a typical batch reaction with the $PtSn_2$/C catalyst is below 40%, and it appears that maintaining low ethylene pressure is beneficial to selectivity towards olefins. When extending the reaction to 70 hours, selectivity of the $PtSn_2$/C drops further to only 27%, and olefin yields are lower than after 22 hours, as the olefins are formed more slowly than they are converted to alkylaromatics. It is clear that significantly improved turnover numbers can be obtained by using this continuous set-up, although eventual catalyst deactivation appears inevitable, limiting the reaction to relatively low olefin yields. For $PtSn_2$/C, these results show that gradual deactivation also occurs, albeit

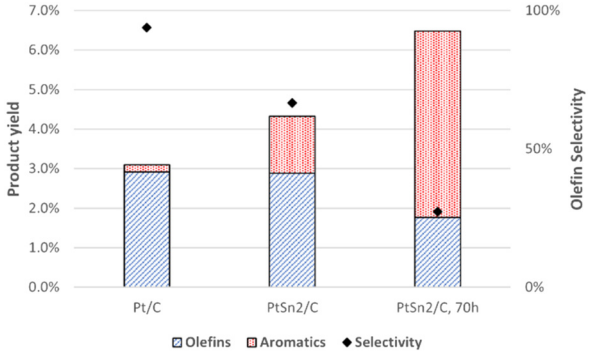

Fig. 8 GC yield of C_{14} products (olefins and alkylaromatics) and selectivity towards olefins. Reaction conditions: 0.05 mmol Pt in 10 ml *n*-tetradecane (38.4 mmol), 250 °C, 0.1 ml_n min^{-1} ethylene (0.26 mmol h^{-1}).

more slowly than for Pt/C. The decrease in olefin yield between 22 and 70 hours also indicates that the reaction rate for further dehydrogenation and aromatization of olefins becomes higher than for the dehydrogenation of alkanes. This may indicate that significant active surface area is maintained for this catalyst, but competitive adsorption between the alkane and dehydrogenated products favors the consecutive conversion of product olefins.

As Pt/C still shows deactivation, despite minimal presence of ethylene, other mechanisms must be at work. Reactions were limited to 30 minutes, and different concentrations of 1-dodecene were added, as a mimic of reaction products. To prevent hydrogenation of dodecene, the reactor was cooled down and briefly opened after catalyst activation under hydrogen, to allow addition of dodecene. The reactor was then heated to the reaction temperature under nitrogen before adding 1 bar of ethylene. Based on previous results, 1-dodecene concentrations up to 3 mol% relative to tetradecane were used. From the results, shown in Fig. 9, it becomes clear that the presence of product olefins is at least partially responsible for the observed deactivation behavior. At low product concentrations (0.1 mol%), ethylene hydrogenation is not significantly slower than in the absence of 1-dodecene, but its rate decreases rapidly as product concentration is increased to 0.5 and 1 mol%. At a concentration of 3 mol%, the rate of hydrogenation is reduced to only 23% of the rate in absence of product olefins.

Surprisingly, tetradecene formation appears to increase significantly as 1-dodecene concentration increases to 1 mol%,

Table 3 Ethylene conversion for reactions under continuous ethylene flow. Reaction conditions: 0.05 mmol Pt in 10 ml *n*-tetradecane (38.4 mmol), 250 °C, 0.1 ml_n min^{-1} ethylene (0.26 mmol h^{-1})

Experiment	Final C_2H_4 conversion[a]	Total C_2H_4 consumption[b] (mmol)	Total C_2H_4 added (mmol)	Overall C_2H_4 conversion
Pt/C–22 h	10%	1.4	5.72	25%
$PtSn_2$/C–22 h	55%	3.3	5.72	58%
$PtSn_2$/C–70 h	30%	7.92	18.2	43%

[a] Determined *via* FTIR analysis of gas sample at reactor outlet at the end of the reaction. [b] Calculated from GC yield of unsaturated C_{14} products.

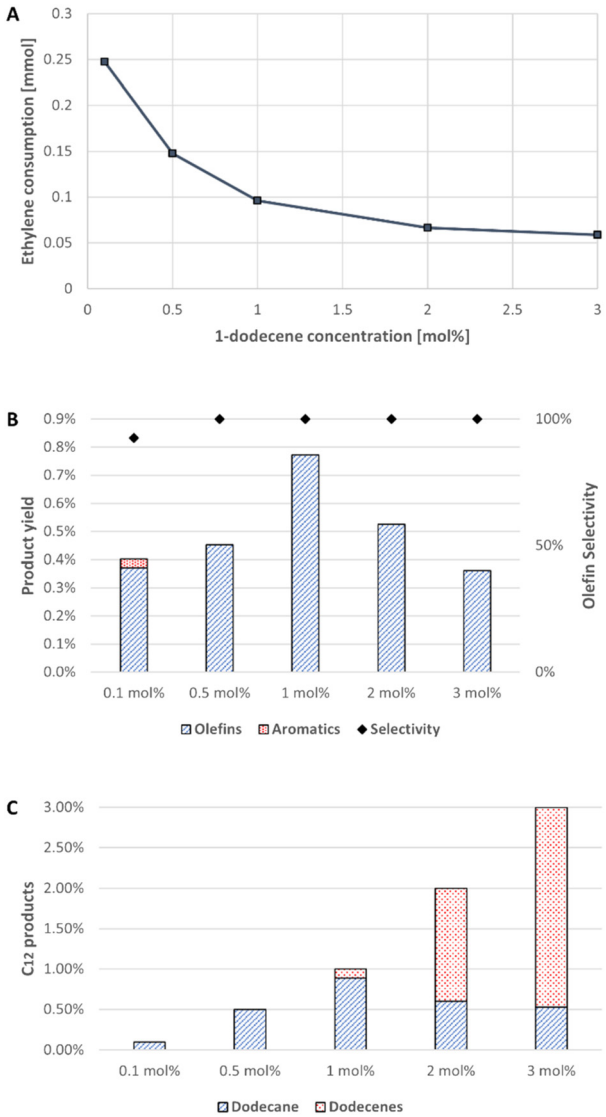

Fig. 9 A) Initial ethylene consumption over 5 wt% Pt/C at different starting concentrations of 1-dodecene, relative to *n*-tetradecane. B) GC yield of C_{14} products (olefins and alkylaromatics) and selectivity towards olefins. C) GC yield of C_{12} products (alkane and olefins). Reaction conditions: 0.05 mmol Pt in 10 ml *n*-tetradecane (38.4 mmol) with 0.1–3 mol% 1-dodecene, 250 °C, 1 bar ethylene at t = 0 (1.15 mmol), 0.5 h.

before gradually decreasing again. This additional tetradecene formation is the result of a hydrogen transfer reaction between tetradecane and dodecene (Fig. 9C). At 0.1 and 0.5 mol%, only dodecane is observed as a C_{12} product, as 1-dodecene is fully consumed as a hydrogen acceptor alongside ethylene. At 1 mol% 1-dodecene, 0.89 mol% dodecane is still detected in the product, decreasing to only 0.53 mol% dodecane at a starting concentration of 3 mol% 1-dodecene. The remaining dodecene is present as a mixture of linear isomers. The analysis of the liquid phase is more complex and less reliable in these reactions, due to overlapping peaks of C_{12} alkylaromatics and C_{14} olefins. Discrepancies in the hydrogen balance can then likely be attributed to the signal of some C_{12} aromatics being included in tetradecene concentrations. Based on these results, product olefins can be seen to retard the transfer dehydrogenation reaction in multiple ways. At low concentrations, the catalyst remains active for alkane dehydrogenation, but product olefins act as alternative hydrogen acceptors, resulting in unproductive transfer reactions. This is clearly seen from the rapid conversion of dodecenes, in combination with rapidly decreasing ethylene conversion. At higher concentrations, however, alkane dehydrogenation slows down, likely due to competitive adsorption of the olefins and possible irreversible adsorption and decomposition. The observed product inhibition is most likely responsible for the inevitable deactivation of Pt catalysts, even at optimal ethylene pressure.

Although catalyst deactivation due to ethylene adsorption and product inhibition appear to limit the conversion of alkanes, the appreciable catalytic activity of supported Pt catalysts warrants further investigation. Optimization of the catalyst composition and support is currently underway, and may yield further improvements to catalyst activity and product yields.

Conclusions

Platinum and platinum-tin catalysts supported on activated carbon were investigated for their potential in the catalytic transfer dehydrogenation of long-chain alkanes. Ethylene was shown to be a viable hydrogen acceptor, allowing for significant alkane dehydrogenation at mild temperatures. Tin-promoted catalysts were found to decrease catalyst deactivation and greatly increase the apparent activation energy of the reaction, in accordance with literature, while also causing an unexpected increase in aromatization activity. Although olefins were the main focus of this work, the dialkylaromatics formed as the main by-product could have applications in *e.g.* detergent manufacturing. The ethylene pressure during the reaction was found to have a strong influence on both the initial catalyst activity and early catalyst deactivation. Ideally, ethylene pressure is to be kept low, to prevent excessive adsorption and the formation of ethylidyne and carbon species, which are likely responsible for significant catalyst deactivation. This was achieved by utilizing a continuous flow of ethylene, based on the expected rate of ethylene consumption, which allowed for an increase in turnover number by a factor of three. However, the catalyst eventually deactivates due to build-up of dehydrogenated products which compete with the alkane for active sites and may adsorb irreversibly or form coke.

Despite its current limitations, the heterogeneously catalyzed transfer dehydrogenation allows for significant alkane dehydrogenation at mild temperatures using simple and widely available catalysts and ethylene as an abundant and convenient hydrogen acceptor. Given the versatility of olefins as intermediates in chemical synthesis, this reaction could have considerable potential as a crucial element of multi-step or tandem processes starting from simple alkanes, or even polyolefins.

Conflicts of interest

The authors declare no conflicts of interests.

Acknowledgements

T. de la Croix gratefully acknowledges the support of the Flanders Research Foundation (FWO) under project 11F6622N. D. De Vos is grateful to FWO for support of project G0D3721N, and to KU Leuven for the iBOF project 21/016/C3. S. Bals and N. Claes acknowledge funding from the European Research Council under the European Union's Horizon 2020 research and innovation program (ERC Consolidator Grant No. 815128- REALNANO). W. Thielemans and S. Eyley thank KU Leuven (grant C14/18/061) and FWO (G0A1219N) for financial support.

Notes and references

1 Y. Zhang, W. Yao, H. Fang, A. Hu and Z. Huang, Catalytic alkane dehydrogenations, *Sci. Bull.*, 2015, **60**, 1316–1331.
2 M. Findlater, J. Choi, A. S. Goldman and M. Brookhart, *Alkane Dehydrogenation*, Springer, Dordrecht, 2012, pp. 113–141, DOI: **10.1007/978-90-481-3698-8_4**.
3 M. M. Bhasin, J. H. McCain, B. V. Vora, T. Imai and P. R. Pujadó, Dehydrogenation and oxydehydrogenation of paraffins to olefins, *Appl. Catal., A*, 2001, **221**, 397–419.
4 J. J. H. B. Sattler, J. Ruiz-Martinez, E. Santillan-Jimenez and B. M. Weckhuysen, Catalytic dehydrogenation of light alkanes on metals and metal oxides, *Chem. Rev.*, 2014, **114**, 10613–10653.
5 W. Won, K. S. Lee, S. Lee and C. Jung, Repetitive control and online optimization of Catofin propane process, *Comput. Chem. Eng.*, 2010, **34**, 508–517.
6 M. Huš, D. Kopač and B. Likozar, Kinetics of non-oxidative propane dehydrogenation on Cr2O3 and the nature of catalyst deactivation from first-principles simulations, *J. Catal.*, 2020, **386**, 126–138.
7 W.-Z. Lang, C.-L. Hu, L.-F. Chu and Y.-J. Guo, Hydrothermally prepared chromia-alumina (xCr/Al 2 O 3) catalysts with hierarchical structure for propane dehydrogenation, *RSC Adv.*, 2014, **4**, 37107–37113.
8 T. V. Voskoboynikov, D. H. Wei, J. W. A. Sachtler and B. V. Vora, US6756340B2, 2004, Dehydrogenation catalyst composition, **https://patents.google.com/patent/US6756340B2/en?oq=+US+Patent+6756340**.
9 M. E. Olbrich, Group VIII catalyst supported on mixture of zinc aluminate and calcium aluminate, 1991.
10 K.-J. Muller-Engel and P. Zehner, Method for the dehydrogenation of hydrocarbons, 2001.
11 G. Wang, X. Zhu and C. Li, Recent Progress in Commercial and Novel Catalysts for Catalytic Dehydrogenation of Light Alkanes, *Chem. Rec.*, 2020, **20**, 604–616.
12 C. Li and G. Wang, Dehydrogenation of light alkanes to mono-olefins, *Chem. Soc. Rev.*, 2021, **50**, 4359–4381, DOI: **10.1039/d0cs00983k**.
13 G. Wang, S. Zhang, X. Zhu, C. Li and H. Shan, Dehydrogenation versus hydrogenolysis in the reaction of light alkanes over Ni-based catalysts, *J. Ind. Eng. Chem.*, 2020, **86**, 1–12.
14 S. He, *et al.*, Kinetics of long chain n-paraffin dehydrogenation over a commercial Pt-Sn-K-Mg/γ-Al2O3 catalyst: Model studies using n-dodecane, *Appl. Catal., A*, 2019, **579**, 130–140.
15 R. Grabowski, Kinetics of Oxidative Dehydrogenation of C_2-C_3 Alkanes on Oxide Catalysts, *Catal. Rev.*, 2006, **48**(2), 199–268, DOI: **10.1080/01614940600631413**.
16 J. M. Venegas, W. P. McDermott and I. Hermans, Serendipity in Catalysis Research: Boron-Based Materials for Alkane Oxidative Dehydrogenation, *Acc. Chem. Res.*, 2018, **51**, 2556–2564.
17 S. Wang and Z. H. Zhu, Catalytic conversion of alkanes to olefins by carbon dioxide oxidative dehydrogenation - A review, *Energy Fuels*, 2004, **18**, 1126–1139.
18 M. Gupta, C. Hagen, R. J. Flesher, W. C. Kaska and C. M. Jensen, A highly active alkane dehydrogenation catalyst: Stabilization of dihydrido rhodium and iridium complexes by a P-C-P pincer ligand, *Chem. Commun.*, 1996, 2083–2084, DOI: **10.1039/CC9960002083**.
19 S. Morisako, *et al.*, Synthesis of A Pincer-IrV Complex with A Base-Free Alumanyl Ligand and Its Application toward the Dehydrogenation of Alkanes, *Angew. Chem., Int. Ed.*, 2019, **58**, 15031–15035.
20 D. Bézier and M. Brookhart, Transfer dehydrogenations of Alkanes and related reactions using iridium pincer complexes, *Top. Organomet. Chem.*, 2016, **56**, 189–208.
21 A. Kumar, *et al.*, Dehydrogenation of n-Alkanes by Solid-Phase Molecular Pincer-Iridium Catalysts. High Yields of α-Olefin Product, *J. Am. Chem. Soc.*, 2015, **137**, 9894–9911.
22 S. Kundu, T. W. Lyons and M. Brookhart, Synthesis of piperylene and toluene via transfer dehydrogenation of pentane and pentene, *ACS Catal.*, 2013, **3**, 1768–1773.
23 R. H. Crabtree, J. M. Mihelcic and J. M. Quirk, Iridium Complexes in Alkane Dehydrogenation, *J. Am. Chem. Soc.*, 1979, **101**, 7738–7740.
24 S. Kumagai and T. Yoshioka, Feedstock recycling via waste plastic pyrolysis, *J. Jpn. Pet. Inst.*, 2016, **59**, 243–253, DOI: **10.1627/jpi.59.243**.
25 R. Miandad, M. A. Barakat, A. S. Aburiazaiza, M. Rehan and A. S. Nizami, Catalytic pyrolysis of plastic waste: A review, *Process Saf. Environ. Prot.*, 2016, **102**, 822–838, DOI: **10.1016/j.psep.2016.06.022**.
26 D. Zhao, X. Wang, J. B. Miller and G. W. Huber, The Chemistry and Kinetics of Polyethylene Pyrolysis: A Process to Produce Fuels and Chemicals, *ChemSusChem*, 2020, **13**, 1764–1774.
27 G. Celik, R. M. Kennedy, R. A. Hackler, M. Ferrandon, A. Tennakoon, S. Patnaik, A. M. LaPointe, S. C. Ammal, A. Heyden, F. A. Perras, M. Pruski, S. L. Scott, K. R. Poeppelmeier, A. D. Sadow and M. Delferro, Upcycling Single-Use Polyethylene into High-Quality Liquid Products, *ACS Cent. Sci.*, 2019, **5**(11), 1795–1803, DOI: **10.1021/acscentsci.9b00722**.

28 J. E. Rorrer, G. T. Beckham and Y. Román-Leshkov, Conversion of Polyolefin Waste to Liquid Alkanes with Ru-Based Catalysts under Mild Conditions, *JACS Au*, 2021, **1**, 8–12.
29 A. Tennakoon, *et al.*, Catalytic upcycling of high-density polyethylene via a processive mechanism, *Nat. Catal.*, 2020, **3**, 893–901.
30 C. Wang, *et al.*, Polyethylene Hydrogenolysis at Mild Conditions over Ruthenium on Tungstated Zirconia, *JACS Au*, 2021, **1**, 1422–1434.
31 M. Sun, *et al.*, Efficient upgrading of polyolefin plastics into C5–C12 gasoline alkanes over a Pt/W/Beta catalyst, *Sustainable Energy Fuels*, 2020, **6**, 271–275.
32 L. D. Ellis, *et al.*, Tandem Heterogeneous Catalysis for Polyethylene Depolymerization via an Olefin-Intermediate Process, *ACS Sustainable Chem. Eng.*, 2021, **9**, 623–628.
33 X. Jia, C. Qin, T. Friedberger, Z. Guan and Z. Huang, Efficient and selective degradation of polyethylenes into liquid fuels and waxes under mild conditions, *Sci. Adv.*, 2016, **2**, 1–8.
34 F. Zhang, *et al.*, Polyethylene upcycling to long-chain alkylaromatics by tandem hydrogenolysis/aromatization, *Science*, 2020, **370**, 437–441.
35 M. Zeng, Y.-H. Lee, G. Strong, A. M. LaPointe, A. L. Kocen, Z. Qu, G. W. Coates, S. L. Scott and M. M. Abu-Omar, Chemical Upcycling of Polyethylene to Value-Added α, ω-Divinyl-Functionalized Oligomers, *ACS Sustainable Chem. Eng.*, 2021, **9**(41), 13926–13936, DOI: **10.1021/acssuschemeng.1c05272**.
36 R. J. Conk, *et al.*, Catalytic deconstruction of waste polyethylene with ethylene to form propylene, *Science*, 2020, **377**, 1561–1566.
37 N. M. Wang, G. Strong, V. DaSilva, L. Gao, R. Huacuja, I. A. Konstantinov, M. S. Rosen, A. J. Nett, S. Ewart, R. Geyer, S. L. Scott and D. Guironnet, Chemical Recycling of Polyethylene by Tandem Catalytic Conversion to Propylene, *J. Am. Chem. Soc.*, 2022, **144**(40), 18526–18531, DOI: **10.1021/JACS.2C07781**.
38 R. Antunes, R. Steiner, L. Marot and E. Meyer, Decomposition studies of NH3 and ND3 in presence of H2 and D2 with Pt/Al2O3 and Ru/Al2O3 catalysts, *Int. J. Hydrogen Energy*, 2020, **47**, 14130–14140.
39 M. P. Seah, Simple universal curve for the energy-dependent electron attenuation length for all materials, *Surf. Interface Anal.*, 2012, **44**, 1353–1359.
40 M. P. Seah, A system for the intensity calibration of electron spectrometers, *J. Electron Spectrosc. Relat. Phenom.*, 1995, **71**, 191–204.
41 J. E. Rorrer, C. Troyano-Valls, G. T. Beckham and Y. Román-Leshkov, Hydrogenolysis of Polypropylene and Mixed Polyolefin Plastic Waste over Ru/C to Produce Liquid Alkanes, *ACS Sustainable Chem. Eng.*, 2021, **9**, 11661–11666.
42 M. Vaarkampa, J. T. Millerb, F. S. Modicab, G. S. Laneb and D. C. Koningsbergerc, The relation between catalytic and elecfronic properties of supported platinum catalysts: the local density of states as determined by x-ray absorition spectroscopy. in.
43 A. Y. Stakheev and L. M. Kustov, Effects of the support on the morphology and electronic properties of supported metal clusters: modern concepts and progress in 1990s, *Appl. Catal., A*, 1999, **188**, 3–35.
44 F. Rodriguez-Reinoso, The role of carbon materials in heterogeneous catalysis, *Carbon*, 1998, **36**, 159–175.
45 H. Jiintgen, Activated carbon as catalyst support: A review of new research results, *Fuel*, 1986, **65**, 1436–1446.
46 I. Horiuti and M. Polanyi, Exchange reactions of hydrogen on metallic catalysts, *Trans. Faraday Soc.*, 1934, **30**, 1164–1172.
47 B. Brandt, *et al.*, Isomerization and hydrogenation of cis-2-butene on Pd model catalyst, *J. Phys. Chem. C*, 2008, **112**, 11408–11420.
48 J. Nam and F. E. Celik, Effect of Tin in the Bulk of Platinum–Tin Alloys for Ethane Dehydrogenation, *Top. Catal.*, 2020, **63**, 700–713.
49 M. L. Yang, Y. A. Zhu, X. G. Zhou, Z. J. Sui and D. Chen, First-principles calculations of propane dehydrogenation over PtSn catalysts, *ACS Catal.*, 2012, **2**, 1247–1258.
50 Y.-L. Tsai, C. Xu and B. E. Koel, Chemisorption of ethylene, propylene and isobutylene on ordered Sn/Pt(111) surface alloys, *Surf. Sci.*, 1997, **385**, 37–59.
51 F. Bortoloti, A. C. Garcia and A. C. D. Angelo, Electronic effect in intermetallic electrocatalysts with low susceptibility to CO poisoning during hydrogen oxidation, *Int. J. Hydrogen Energy*, 2015, **40**, 10816–10824.
52 J. H. Kim, *et al.*, Influence of Sn content on PtSn/C catalysts for electrooxidation of C1–C3 alcohols: Synthesis, characterization, and electrocatalytic activity, *Appl. Catal., B*, 2008, **82**, 89–102.
53 G. J. Siri, *et al.*, XPS and EXAFS study of supported PtSn catalysts obtained by surface organometallic chemistry on metals, *Appl. Catal., A*, 2005, **278**, 239–249.
54 L. Nykänen and K. Honkala, Density functional theory study on propane and propene adsorption on Pt(111) and PtSn alloy surfaces, *J. Phys. Chem. C*, 2011, **115**, 9578–9586.
55 J. M. Essen, J. Haubrich, C. Becker and K. Wandelt, Adsorption of ethene on Pt(1 1 1) and ordered Pt_xSn/Pt(1 1 1) surface alloys: A comparative HREELS and DFT investigation, *Surf. Sci.*, 2007, **601**(16), 3472–3480, DOI: **10.1016/j.susc.2007.06.037**.
56 H. Dong, Y.-C. Chen and C. Feldmann, Polyol synthesis of nanoparticles: status and options regarding metals, oxides, chalcogenides, and non-metal elements, *Green Chem.*, 2015, **17**, 4107–4132, DOI: **10.1039/C5GC00943J**.
57 M. A. Stranick and A. Moskwa, SnO by XPS, *Surf. Sci. Spectra*, 1993, **2**, 45–49.
58 G. J. Siri, *et al.*, XPS and EXAFS study of supported PtSn catalysts obtained by surface organometallic chemistry on metals: Application to the isobutane dehydrogenation, *Appl. Catal., A*, 2005, **278**, 239–249.
59 D. Godbey, F. Zaera, R. Yeates and G. A. Somorjai, Hydrogenation of chemisorbed ethylene on clean, hydrogen, and ethylidyne covered platinum (111) crystal surfaces, *Surf. Sci.*, 1986, **167**, 150–166.

60 F. B. Passos, M. Schmal and M. A. Vannice, Ethylene Adsorption on Al2O3-Supported Pt, Pt–Sn, and Pt–In Catalysts, *J. Catal.*, 1996, **160**, 118–124.
61 A. Palazov, *et al.*, Adsorption and hydrogenation of ethylene, 1-hexene, and benzene and CO adsorption on PtAl2O3 and PtSnAl2O3 catalysts, *J. Catal.*, 1987, **103**, 249–260.
62 B. Khanh Vu, *et al.*, Electronic density enrichment of Pt catalysts by coke in the propane dehydrogenation, *Korean J. Chem. Eng.*, 2011, **28**, 383–387.